Optimized structural parameters and heat extraction capacity of mixing device for constant pressure CO2 mineralization using alkaline waste

Wei Lu
Shandong University of Science and Technology
Yang Yuan
Shandong University of Science and Technology
Xiangming Hu
Shandong University of Science and Technology
Guansheng Qi (qgs_fire@sdust.edu.cn)
Shandong University of Science and Technology
Lulu Sun
Shandong University of Science and Technology
Maoyuan Zhang
Shandong University of Science and Technology
Mingjun Wang
Shandong University of Science and Technology
Min He
Shandong University of Science and Technology

Research Article

Keywords: Alkaline waste, CO2 mineralization, Mixing device, Structural parameters, Reaction heat extraction

Posted Date: April 5th, 2022

DOI: https://doi.org/10.21203/rs.3.rs-1426286/v1

Abstract

Alkaline waste such as calcium carbide slag is an ideal material for mineralizing CO_2 and promoting atmospheric carbon reduction. In this study, the structural parameters of a mixing device and a thermal extraction method for the high-efficiency mineralization of CO_2 using alkaline waste were optimized. First, the effects of various factors including the length–diameter ratio, blade inclination angle, spacing, and diameter in constant-pressure and continuous-feed systems on the degree of CO_2 mineralization using carbide slag and on the extraction of the reaction heat during the mineralization process were investigated through experiments and numerical simulations. The influence of different configurations of the heat pipe and the internal fluid flow rate on extraction of the reaction heat was explored. The influence of different factors on the mineralization efficiency and heat extraction ability was analyzed based on the orthogonal simulation method. When the length–diameter ratio, blade inclination angle, spacing, and diameter of the mixing device were 3, 15, 6 cm, and 14 cm respectively, and a heat pipe was used, the heat extraction during calcium carbide slag (alkaline waste) mineralization of CO_2 was at a maximum. In addition, the winding configuration of the heat pipe, which is beneficial for extracting more reaction heat, was optimal, and a model of the relationship between the heat pipe outlet water temperature and flow velocity at the outlet of the heat pipe was established. This study provides theoretical guidance for the field application of alkaline waste for high-efficiency mineralization of CO_2, which can accelerate the realization of peak CO_2 emissions and carbon neutrality.

1. Introduction

Mixing technology is widely used in the desalination of seawater, chemical and metallurgical processing, and other industrial processes (Mauro et al 2010; Li et al 2017). With the increasing industrial demand for ethylene production and coal and iron resource mining, a large amount of alkaline waste is produced, such as calcium carbide slag and fly ash (Miao et al 2022; Wu et al 2021a). At the same time, many of the alkaline components in these wastes can mineralize and sequester large amounts of CO_2 (Mayoral et al 2021; Yang et al 2019; Wang et al 2021). A mixing device that can ensure that the alkaline waste mineralizes and absorbs a large amount of CO_2 and that can efficiently extract a large amount of reaction heat can accelerate the realization of peak CO_2 emissions and carbon neutrality (Dar et al 2021).

Improving the efficiency of the mixing device is imperative for the efficient mineralization of CO_2 using alkaline waste, where the structural parameters of the mixing device are known to affect its efficiency (Geng et al 2021). Methods of achieving efficient mass and heat transfer in mixing devices have been widely studied in scholastic settings. For example, Moradkhani et al (2017). studied the influence of five impeller structures and three different aeration flow rates on the mass transfer coefficient based on the "k-ε" Reynolds-averaged Navier-Stokes (RANS) model. They found that a stirring speed of 300–800 rpm provided the most effective rate of oxygen mass transfer in a two-phase distribution bioreactor. Tatterson et al (1987). studied the length–diameter ratio of the agitator in a mixing device and found that when the length–diameter ratio was greater than 4, the hydrodynamics of the fluid near the blade was close to solid rotation. Ranade and Joshi (1989) studied the influence of the blade inclination on the flow pattern in a mixing device

and determined that the blade inclination has a significant effect on the flow characteristics. Ameur (2016) found that the stirring power increases with an increase in the blade inclination angle. Wu et al. (2021b) studied the heat transfer performance of a rotating fluidized bed using the Euler-Lagrangian hybrid method. It was found that the heat transfer coefficient of the bed wall increased by 20% when the blade inclination angle was changed from 45° to 12°.

Kumaresan et al. (2016) obtained a higher average shear rate, average normal stress, and turbulent kinetic energy of a downflow impeller by studying the influence of the blade inclination angle on the power. Zuo et al. (2020) studied the effect of different blade numbers on the mixing efficiency of an agitator using the discrete element method, and found that increasing the blade number can promote the mixing efficiency. Bao et al. (2020) used the discrete element method to study the effect of the impeller structure on particle flow and mixing. The results showed that the mixing efficiency and axial diffusion coefficient increased with an increase in the blade diameter.

Different from previous studies (Yuan et al. 2022), this paper mainly studies the effect of mixing devices with different structural parameters on thermal extraction efficiency. In addition, heat extraction by the heat pipe using different winding configurations is studied. The heat extraction ability of the heat pipe at different fluid velocities is analyzed. Despite numerous studies on the structural parameters of mixing devices, there are few studies of the influence of the length–diameter ratio, blade inclination angle, blade diameter, and blade spacing on the reaction heat transfer and heat transfer efficiency. In order to realize high efficiency and maximize the mineralization and storage of CO_2 using waste, it is urgent to develop a device for the rapid mineralization of CO_2. Therefore, in this study, the influence of various factors, including the length–diameter ratio of the mixing device, inclination angle, spacing, and diameter of the blades, on the degree of CO_2 mineralization using carbide slag (where the mineralization degree refers to the ratio of the mass of carbide slag participating in the CO_2 mineralization reaction to the total mass of carbide slag filled into the mixing device) and reaction heat extraction during the mineralization process are investigated through experiments and numerical simulations. The relationship between the heat pipe outlet water temperature and fluid velocity at the outlet of the heat pipe is analyzed by numerical simulation.

This research is of great significance for the early realization of peak CO_2 emissions and carbon neutrality, and enhance the extraction and utilization of reaction heat during the mineralization process (Pan et al 2020). In Section 2, the mechanism of CO_2 mineralization with carbide slag is analyzed, and a mathematical model of CO_2 mineralization with carbide slag slurry under constant pressure is established and verified. In Section 3, a mixing device model with different structural parameters is established and the effects of different structural parameters on the degree of mineralization and reaction heat extraction under constant-pressure and continuous-feed conditions are studied by numerical simulation. a model of the relationship between the heat pipe outlet water temperature and flow velocity at the outlet of the heat pipe is established.

2. Mechanism Of Co2 Mineralization And Mathematical Model

2.1 Mechanism of CO_2 mineralization

CO_2 is converted to the liquid phase through the gas/liquid interface, and the large CO_2 bubbles are broken into small bubbles by the rotating blades. Thereafter, CO_2 reacts with H_2O to form H_2CO_3. Finally, the CO_3^{2-} formed by ionization of H_2CO_3 combines with the Ca^{2+} ions formed from the carbide slag slurry to generate $CaCO_3$ as a precipitate (Wylock et al 2010). Figure 1 shows a schematic of the instantaneous mass transfer near the gas-slurry interface of the carbide slag slurry.

The total reaction during CO_2 absorption by the carbide slag slurry can be expressed as Eq. (1) (Meng et al. 2022; Liu et al. 2021):

$$Ca(OH)_2(s) + CO_2(g) = Ca(CO)_3(s) + H_2O(l)$$

1

Reaction (1) occurs at a high rate in the temperature range of 25–100 ℃ and involves many individual reactions, such as the generation and ionization of H_2CO_3, the data acquired using the pH meter revealed that the pH of the carbide slag slurry was in the range of 12–14. When the pH is greater than 11, reactions (1) are expected to occur at a high rate (Gupta et al 2002). Therefore, the process of CO_2 absorption by calcium carbide slag slurry can be replaced by reaction (1) (Rigopoulos et al. 2003).

2.2 Mathematical model of CO_2 mineralization under constant pressure

The motion of a fluid should satisfy the basic laws of fluid mechanics, physics, and chemistry, that is, the laws of conservation of mass, momentum, and energy (Darmana et al. 2007). Therefore, in this study, the process of CO_2 absorption by calcium carbide slag at constant pressure was numerically simulated according to the following three governing equations: the continuity equation, momentum equation, and energy conservation equation, the equations used to establish the mathematical model in this study are shown in Table 1:

Table 1
equation used in mathematical model

Items	Equations
continuity equation (Wang et al. 2021; Pham et al. 2022)	$\frac{\partial}{\partial t}\left(\alpha_j\rho_j\right)+\nabla\bullet\left(\alpha_j\rho_j\vec{v}_j\right)=-m_{j\to l}$
momentum equation (Song et al. 2021; Zhang et al. 2016)	$\frac{\partial}{\partial t}\left(\alpha_j\rho_j\vec{v}_j\right)+\nabla\bullet\left(\alpha_j\rho_j\vec{v}_j\vec{v}_j\right)=-\alpha_j\nabla\bullet\rho_j+\alpha_j\rho_j\mathrm{G}+\nabla\bullet\left(\alpha_j\gamma_j\right)+M_j-m_{j\to l}\vec{v}_j$
energy equation (Hua et al. 2021; Liu et al. 2020)	$\frac{\partial}{\partial t}\left(\alpha_j\rho_j\vec{v}_j\right)+\nabla\bullet\left(\alpha_j\rho_j\vec{v}_j\left(h_j+p_j\right)\right)=\nabla\bullet\left(\alpha_j\vec{v}_j\gamma_j\right)-\nabla\bullet\vec{q}_j+S_{e,j}-m_{j\to l}\vec{v}_j$
Material transport equation (Heydarifard et al. 2020)	\frac{\partial }{\partial t}\left({\alpha }_{j}{\rho }_{j}{Y}_{j}^{i}\right)+\nabla \bullet {\alpha }_{j}{\rho }_{j}{\overrightarrow{v}}_{j}{Y}_{j}^{i}=-{\overrightarrow{J}}_{j}^{i}+{D}_{j}^{i}+{S}_{j}^{i}
pressure strain equation (Heydarifard et al. 2020)	{\gamma }_{j}=-{\mu }_{j}(\nabla {\overrightarrow{v}}_{j}+{(\nabla {\overrightarrow{v}}_{j})}^{T}-\frac{2}{3}I\nabla {\overrightarrow{v}}_{j})
chemical reaction Equation (Mondal et al. 2017)	$K=AT^{\beta}e^{-E_a/RT}$

The CO_2 source phase was set at the point of entry of CO_2. Because reaction (1) is very fast, it is considered that the volume fraction of CO_2 dissolved in water is constant, which ensures that the entire reaction process is completed under constant pressure.

Different turbulence models produce significantly different results. Herein, complex fluid movements were considered, such as high-speed rotation of the blades. To realize high-precision simulation of CO_2 mineralization by calcium carbide slag, the realizable k- ε model with higher precision and applicable range was selected (Raj et al. 2020). The SIMPLE algorithm with good convergence under small time steps was adopted, which can conserve computer resources to a certain extent (Ijaz et al. 2007). The detailed parameter settings in numerical simulation are listed in Table 2.

Table 2
Parameter setting in numerical simulation.

Parameter setting	Type	
Solution setting	Energy equation	Open (1,2)
	Turbulence model	Realizable k-ε model (1,2)
	Chemical reaction	Component transportation model (1,2)
	Energy equation	Open (1,2)
	Rotation	Sliding mesh (1,2)
	Solution method	Simple (1,2)
Boundary condition	Initial temperature	300 K (1,2)
	Wall	Heat flux
	Inlet	Speed-inlet (2)
	Outlet	Pressure-outlet (2)
	Wall surface of heat pipe	Coupling heat transfer (1,2)

Note: (1) indicates the parameter setting for CO_2 mineralization in the constant-pressure and closed system, and (2) indicates the parameter setting for CO_2 mineralization in the constant-pressure and continuous-feed system. The heat pipe was made of copper.

2.3 Verification of validity of the numerical simulation method

The validity of the mathematical model used in this paper has been verified in previous studies (Yuan et al. 2022). The maximum errors between simulated mineralization degree results and experimental data is less than 10% (**Fig. 2**), which indicates that the mathematical model constructed is effective in simulating the process of CO_2 mineralization with carbide slag (Malakhov et al.2020). Therefore, the mineralization process of CO_2 in stirring devices with different structural parameters is studied next.

3. Numerical Simulation Of Co2 Mineralization Process In Mixing Device

3.1 Numerical simulation of CO_2 mineralization using calcium carbide slag and optimum process parameters

The mass transfer and heat pipe outlet water temperature for CO_2 mineralization with calcium carbide slag were studied by controlling the length-to-diameter ratio (A), blade inclination angle (B), blade spacing (C), and blade diameter (D) in the device. The numerical simulation was carried out by designing orthogonal experiments, and the gradient was divided, as shown in Table 3. The 3D physical model of the mixing device centered on (0,0,0) was established using Solidworks software (Fig. 3). The model includes a slurry inlet and

outlet, a CO_2 source phase, and a heat pipe (screw thread spacing of 10 cm), The data from domestic and foreign studies on the degree of mineralization promoted by different factors were summarized, from which the rotational speed, pressure, solid–liquid ratio, and slurry entry speed were set to 2000 rpm, 5 Mpa, 0.25, and 0.8 m/s, respectively.

The length–diameter ratio, blade angle, spacing, and diameter of the mixing device are 1.5-3, 15–45°, 3–6 cm and 11–14 cm, respectively, and were equally divided into four gradients for orthogonal numerical simulation. The gradient was divided as shown in Table 3.

Table 3
Gradients in the orthogonal simulation.

Group	Factor			
	A	B	C	D
1	1.5	15°	3 cm	11 cm
2	2	25°	4 cm	12 cm
3	2.5	35°	5 cm	13 cm
4	3	45°	6 cm	14 cm
Note: The inlet speed of the heat pipe (water temperature 300 K) was 2 m/s				

The degree of mineralization and the heat pipe outlet water temperature were calculated when the mass of the $CaCO_3$ outlet was stable. Sixteen groups of mineralization degree data and heat pipe outlet water temperature were obtained by orthogonal simulation, as shown in Table 4.

Table 4
Mineralization degree and water temperature after orthogonal simulation.

Group	Factor				Result	
	A	B	C	D	A (%)	T (K)
1	1,600	4.5	0.1	0.2	82.74	303.82
2	1,800	5	0.15	0.2	67.48	305.47
3	2,000	5.5	0.2	0.2	79.02	306.34
4	2,200	6	0.25	0.2	45.59	308.21
5	1,600	5	0.2	0.4	84.59	315.24
6	1,800	4.5	0.25	0.4	82.94	316.20
7	2,000	6	0.1	0.4	81.19	306.21
8	2,200	5.5	0.15	0.4	80.12	308.50
9	1,600	5.5	0.25	0.6	80.90	322.21
10	1,800	6	0.2	0.6	78.13	317.52
11	1,200	4.5	0.15	0.6	76.97	311.54
12	2,200	5	0.1	0.6	80.29	307.23
13	1,600	6	0.15	0.8	78.58	315.50
14	1,800	5.5	0.1	0.8	80.56	309.64
15	2,000	5	0.25	0.8	80.62	322.90
16	2,200	4.5	0.2	0.8	81.79	317.51
K_{11}	81.70	81.11	81.20	68.71		
K_{12}	77.28	78.25	75.79	82.21		
K_{13}	79.45	80.15	80.88	79.07		
K_{14}	71.95	70.87	72.51	80.39		
R_1	9.75	10.24	8.69	13.50		
K_{21}	314.19	312.27	306.73	305.96		
K_{22}	312.21	312.71	310.25	311.54		

Note: *A* is the mineralization degree, and *T* is the water temperature. *Kij* represents the average mineralization degree and outlet temperature rise corresponding to level I in column *j*. R_j stands for $k_{max} - K_{min}$ in column *j*.

Group	Factor				Result	
	A	B	C	D	A (%)	T (K)
K_{23}	311.75	311.67	314.15	314.63		
K_{24}	310.36	311.86	317.38	316.39		
R_2	3.83	1.04	10.65	10.43		
Note: *A* is the mineralization degree, and *T* is the water temperature. *Kij* represents the average mineralization degree and outlet temperature rise corresponding to level I in column *j*. R_j stands for $k_{max} - K_{min}$ in column *j*.						

The range of R_j reflects the influence of this factor on the degree of mineralization or temperature rise. The greater the R_j value, the greater the influence of this factor on the results. As can be seen from Table 4, for the degree of mineralization, R_1 follows the order: A > D > B > C. For the heat pipe outlet water temperature, R_2follows the order: A > D > C > B. Therefore, factor A has the greatest influence on both the degree of mineralization and the heat pipe outlet water temperature.

Table 5
Numerical simulation—Analysis of variance for mineralization degree.

	A	B	C	D	Error
Sum of squared deviation	1831.33	40.31	9.41	190.16	2071.21
Degree of freedom	3.00	3.00	3.00	3.00	12.00
F_{ratio}	3.54	0.08	0.02	0.37	
$F_{critical}$ **(0.05)**	3.49	3.49	3.49	3.49	
Significant	Significant				
Note: F_{ratio} **represents** F **value**, $F_{critical}$ **value (0.05) represents significance level 0.05**					

Table 6
Numerical simulation—Analysis of variance for heat pipe outlet water temperature.

	A	B	C	D	Error
Sum of squared deviation	245.51	3.93	12.48	18.72	280.63
Degree of freedom	3	3	3	3	12.00
F_{ratio}	3.50	0.06	0.18	0.27	
$F_{critical}$ **(0.05)**	3.49	3.49	3.49	3.49	
Significant	Significant				

Combined with the data in Tables 5 and 6, the analysis of variance shows that when the mineralization degree is an objective function (Wu et al. 2020), the F_{ratio} for factors A, B, and D (3.54, 0.08, and 0.37, respectively) is greater than that when the heat pipe outlet water temperature is the objective function (3.50, 0.06, and 0.27, respectively). Thus $A_4B_1D_4$ was selected under the objective function of the mineralization degree. When the heat pipe outlet water temperature is the objective function, the F_{ratio} (0.18) of factors A, B, and D is greater than that when the mineralization degree is the objective function (0.02). Therefore, C_4 was selected as the objective function for the heat pipe outlet water temperature. The optimal combination is $A_4B_1C_4D_4$, that is, the length-to-diameter ratio of the mixing device is 3, and the angle, spacing, and diameter of the blade are 15°, 6 cm, and 14 cm, respectively, which is the fourth group of sixteen orthogonal simulations.

3.2 Analysis of CO_2 mineralization and quantification of heat extraction for mixing device

The length-to-diameter ratio of the mixing device has the greatest influence on the mineralization capacity and the heat pipe outlet water temperature. To a certain extent, increasing the length of the mixing device can increase the contact time between the calcium carbide slag and CO_2, leading to greater reaction, a longer heat exchange time between the heat pipe and the high-temperature slurry in the mixing device, and improved heat exchange efficiency. Group 4 of the numerical simulation data was imported into TECPLOT post-processing software, and the nephograms of the $CaCO_3$ concentration and temperature distribution (after the mass of $CaCO_3$ at the outlet stabilized) were obtained (**Fig. 4**).

The nephograms of the $CaCO_3$ concentration and temperature distribution show that the $CaCO_3$ concentration and temperature were high near the entrance and low near the exit. This is because a large amount of heat is released after the reaction of $Ca(OH)_2$ and CO_2 to form $CaCO_3$, which increases the temperature of the slurry containing $CaCO_3$, resulting in a similar $CaCO_3$ concentration distribution and temperature distribution. Table 4 shows that after the mass of $CaCO_3$ at the outlet stabilized, the degree of mineralization and the temperature of the outlet reached 78% and 319.21 K, respectively. The calculation indicates that the mixing device with the $A_4B_1C_4D_4$ structure parameters can mineralize about 2.14 t of CO_2 and consume 4.53 t carbide slag within one hour, which is equivalent to the CO_2 released by complete combustion of 0.957 t coal. In addition, 2.35 m^3 of water can be heated from 300 K to 319.21 K for the mineralization of 1 t CO_2, where the amount of heat extracted reached 189.60 MJ.

4. Numerical Simulation Of Thermal Extraction Capacity Of Mineralization Unit

4.1 Effect of heat pipe configuration on heat extraction capacity

As shown in Table 4, the simulated mineralization capacity and the heat pipe outlet water temperature were the highest in the fourth group. Therefore, the structural parameters from the fourth group simulation were

used; that is, the length–diameter ratio, blade angle, spacing, and diameter of the mixing device were 3, 15, 6, and 14 cm, respectively. The influence of the winding density of the heat pipe on the heat extraction capacity was investigated. The distance between the outlet and the inlet of the heat pipe in the mixing device was 120 cm, which was divided into **a**, **b**, and **c** regions on average, and the pitch of the three areas was changed from 10 cm to 5 cm to encrypt the heat pipe in the corresponding area, after which the calculation was carried out. The heat pipe outlet water temperatures with different winding densities are shown in Fig. 5.

Figure 5 shows that the heat pipe outlet water temperature was highest when the winding density corresponded to (a). Combined with **Fig. 4(b)**, it can be seen that the reaction heat produced by the reaction of $Ca(OH)_2$ and CO_2 was mainly concentrated in the area of the mixing device. When the winding number of the heat pipe in this area is increased, the heat exchange time between the water inside the heat pipe and the high-temperature slurry outside the heat pipe can be increased, allowing the water inside the heat pipe to absorb more heat, thus increasing the heat pipe outlet water temperature and improving the heat exchange efficiency. Therefore, the winding configuration of the heat pipe (Fig. 5**(a)**) was employed in studying the effect of the flow velocity of the internal liquid on the heat extraction capacity.

4.2 Effect of flow rate on thermal extraction ability

In this section, the variation of the heat pipe outlet water temperature at flow velocities of 0.2–4 m/s in the heat pipe (where the flow velocity refers to the flow velocity in the heat pipe) was studied. After locally encrypting the density of the heat pipe, there were 16 turns of the heat tube in the mixing device. To monitor the real-time change in the heat pipe outlet water temperature, four points **a** (5.24, − 60, 30.69), **b** (0, 50, 21), **c** (0, − 22.5, − 21), and **d** (0, − 55, 21) were set up at lap 2, lap 8.5, lap 15, and at the outlet of the heat pipe when the water enters the mixing device. The temperature change at each point was determined after the mass of $CaCO_3$ at the outlet stabilized. The curve **t** represents the temporal evolution of water flow from the inlet of the heat pipe to the outlet, and the data in curve b corresponds to $\mathbf{T_b}$ = 12 K.

As shown in Fig. 6, the slope of curve **t** decreased gradually overall. As the flow velocity increased, the time for water to flow from the heat pipe inlet to the outlet decreased. The time required for heat exchange between water in the heat pipe and high-temperature calcium carbide slag slurry decreased with an increase in the flow velocity, leading to a less pronounced decrease in the heat exchange capacity. Therefore, the temperature of points **a**, **b**, **c**, and **d** decreased slowly with an increase in the flow velocity, and the extent of the decrease gradually became smaller.

The values $A = 6.77$, $t = 2.67$, and $y_0 = 315.91$ were obtained for the exponential decay by using the Expdecl model ($y = A*exp(x/t) + y_0$) in Origin software to analyze the data in curve **a**. The functional relationship between the heat pipe outlet water temperature and flow velocity at the outlet of the heat pipe is represented by Eq. (2).

$$T=6.77\times \text{e}\text{x}\text{p}(-{\text{V}}_{\text{H}}/2.67)+315.91 \quad (2)$$

The amount of heat extracted from water in the heat pipe in 1 h is related to the increase in the heat pipe outlet water temperature. Therefore, the function Q describing the relationship between the amount of heat

extracted and the flow velocity can be obtained from Eq. (3).

$$Q=[T\left({v}_{H}\right)-300]\times \pi {r}^{2}\times {v}_{H}\times c \quad (3)$$

Here, r is the radius of the heat pipe, t is time, and c is the specific heat capacity of water (4.2×10^3 J/(kg·K)).

From Fig. 7, when the flow velocity is 1 m/s, the heat pipe outlet water temperature is 320.56 K, the heat extraction is 97.66 MJ, and the water output of the heat pipe is 1.13 m^3/h; when the flow velocity is 2 m/s, the heat pipe outlet water temperature is 319.11 K, the heat extraction is 181.50 MJ, and the water output of the heat pipe is 2.26 m^3/h. From comprehensive consideration of the heat pipe outlet water temperature, heat extraction, and water output, 1–2 m/s was selected as an appropriate flow velocity for extracting the reaction heat of the mixing device.

5 Conclusions

The effects of the length–diameter ratio, blade inclination angle, spacing, and diameter on the CO_2 mineralization degree and extraction of the reaction heat using alkaline waste were studied in constant-pressure and continuous-feed systems through experiments and numerical simulations.

(1) Orthogonal numerical simulation showed that when mineralizing CO_2 in the constant-pressure and continuous-feed systems, the influence of the length–diameter ratio, blade inclination angle, spacing, and diameter on the mineralization degree follow the order: length − diameter ratio of mixing device>blade diameter>blade inclination angle>blade spacing. The influence on the heat pipe outlet water temperature follows the order: length − diameter ratio **>** blade diameter **>** blade spacing **>** blade inclination angle.

(2) When the length − diameter ratio, blade inclination angle, spacing, and diameter of the mixing device are 3, 15°, 6 cm, and 14 cm respectively, the amount of heat extracted from CO_2 mineralization using alkaline waste calcium carbide slag and a heat pipe is optimal; that is, 2.14 t CO_2 can be mineralized at most in one hour, and 4.53 t carbide slag is consumed at the same time. The amount of heat extracted from mineralization of 1 t CO_2 reached 189.60 MJ. The study shows that increasing the length-to-diameter ratio of the blade in the mixing device can further improve the degree of mineralization and the thermal extraction ability.

(3) The relationship between the winding mode, flow velocity, and water temperature at the heat pipe outlet was evaluated through numerical simulations, showing that when the left area of the heat pipe was encrypted, more reaction heat could be extracted for utilization. On this basis, a model of the relationship between the water temperature and flow velocity was established. When the flow velocity was 1 − 2 m/s, the heat extraction reached 97.66 − 181.50 MJ, which provides a theoretical basis for the application of the reaction heat extraction in the field.

Abbreviations

Nomenclature	
t	time, s
α_j	volume fraction of jth phase
j	jth phase
ρ	density, kg/m^3
v	velocity vector, m/s
$m_{j\to l}$	mass transfer rate from phase j to phase l
G	gravitational constant, (m·s^{-1})
γ	stress tensor, N/m^2
M_j	the interphase momentum exchange between phase j and other Phase
h	total energy per unit mass, (Nm/kg)
p	pressure, MPa
q	interphase heat exchange, (J/(s·m^3))
S	source term in the species balance equation, (kg/(s·m^3))
μ_j	viscosity, kg/(m·s)
I	ionic concentration, (kmol·m^{-3})
Y	mass fraction
i	substance i in the phase j
J	mass diffusion coefficient of matter
D	net production rate of chemical reaction, (kg/(s·m^3))
K	the rate constant
A	Pre-exponential factor, (unit time^{-1})
T	Temperature, K
β	temperature index
e	natural logarithm
E_a	Activation energy, (j/kgmol)
R	Gas constant, J/(mol·K)

Nomenclature	
v_H	Inlet velocity of heat pipe water, m/s
r	Heat pipe radius,m
c	Specific heat capacity,$4.2\times10^3 j/(kg\cdot K)$

Declarations

Acknowledgments

We like to acknowledge the support of State Key Laboratory of Strata intelligent Control and Green Mining Co-founded by Shandong Province and the Ministry of Science and Technology.

Funding (Not applicable)

This work was supported by the National Natural Science Foundation of China (51804185, 51974178), the Natural Science Foundation of Shandong Province (ZR2019BEE041).

Competing Interests (Not applicable)

The authors declare that they have no known competing financial interests or personal relationships that could have appeared to influence the work reported in this paper.

Author Contributions (Not applicable)

All authors contributed to the study conception and design. Material preparation, data collection and analysis were performed by Wei Lu, Xiangming Hu, Guansheng Qi, Lulu Sun Maoyuan Zhang, MingJun Wang, Min He. The first draft of the manuscript was written by Yang Yuan and all authors commented on previous versions of the manuscript. All authors read and approved the final manuscript. The following are the author's specific contributions.

Credit Author Statement

Author's name	Term	Definition
Wei Lu	1. Investigation 2. Writing-Original Draft 3. Writing-Review& Editing	1.Conducting a research and investigation process, specifically performing the experiments, or data/evidence collection 2.Verification, whether as a part of the activity or separate, of the overall replication/ reproducibility of results/experiments and other research outputs
Yang Yuan	1. Investigation 2. Visualization 3.Writing-Review& Editing	1.Conducting a research and investigation process, specifically performing the experiments, or data/evidence collection 2.Preparation, creation and/or presentation of the published work, specifically writing the initial draft
Xiangming Hu	1. Investigation 2. Resources	1.Provision of study materials, reagents, materials, laboratory samples, animals, instrumentation, computing resources, or other analysis tools
Guansheng Qi	1. Resources 2. Funding acquisition 3. Project administration	1.Acquisition of the financial support for the project leading to this publication 2.Provision of study materials, reagents, materials, laboratory samples, animals, instrumentation, computing resources, or other analysis tools 3.Management and coordination responsibility for the research activity planning and execution
Lulu Sun	1.Investigation 2.Resources	1.Provision of study materials, reagents, materials, laboratory samples, animals, instrumentation, computing resources, or other analysis tools
Maoyuan Zhang	1. Investigation 2. Resources	1.Conducting a research and investigation process, specifically performing the experiments, or data/evidence collection
MingJun Wang	1. Investigation 2. Resources	1.Conducting a research and investigation process, specifically performing the experiments, or data/evidence collection
Min He	1. Investigation 2. Resources	1.Conducting a research and investigation process.

Ethical Approval (Not applicable)

We guarantee that our work is original and has not been submitted to other journals.

Consent to Participate (Not applicable)

All authors contributed to the study conception and design. Material preparation, data collection and analysis were performed by Wei Lu, Xiangming Hu, Guansheng Qi, Lulu Sun Maoyuan Zhang, MingJun Wang, Min He. The first draft of the manuscript was written by Yang Yuan and all authors commented on previous versions of the manuscript. All authors read and approved the final manuscript.

Consent to Publish (Not applicable)

We guarantee that all authors have known and agreed to publish this article in the Journal of environmental science and pollution research

Availability of data and materials (Not applicable)

We guarantee the authenticity and reliability of the data.

References

1. Ameur H (2016) Mixing of complex fluids with flat and pitched bladed impellers: Effect of blade attack angle and shear-thinning behaviour. Food Bioprod Process 99:71–77
2. Bao YY, Li TC, Wang DF, Cai ZQ, Gao ZM (2020) Discrete element method study of effects of the impeller configuration and operating conditions on particle mixing in a cylindrical mixer. Particuology 49:146–158
3. Dar AA, Hameed J, Huo CH, Sarfraz M, Albasher G, Wang CY, Nawaz A (2022) Recent optimization and panelizing measures for green energy projects; insights into CO_2 emission influencing to circular economy. Fuel 314:123094
4. Darmana D, Henket RLB, Deen NG, Kuipers JAM (2007) Detailed modelling ofhydrodynamics, mass transfer and chemical reactions in a bubble column using a discrete bubble model: Chemisorption of CO_2 into NaOH solution, numerical and experimental study. Chem Eng Sci 62:2556–2575
5. Geng SJ, Mao ZS, Huang QS, Chao Y (2021) Process Intensif Pneumatically Agitated Slurry Reactors Eng 7:304–325
6. Gupta H, Fan LS (2002) Carbonation-Calcination Cycle Using High Reactivity Calcium Oxide for Carbon Dioxide Separation from Flue Gas. Ind Eng Chem Res 41:4035–4042
7. Heydarifard M, Ghaemi A, Shirvani M (2020) Numerical simulation of CO_2 chemical absorption in a gas-liquid bubble column using the space-time CESE method. J Environ Chem Eng 8:104111
8. Hua Y, Nie W, Guo LD, Cheng L (2021) The control effect of 3D spiral wind-curtain generator on respirable dust pollution during tunnelling process. Environ Sci Pollut Res 28:68212–68228
9. Ijaz M, Anand NK (2007) Simulation of Unsteady Incompressible Viscous Flow using Higher-Order Implicit RungeKutta Methods—Staggered Grid, Numer. Heat Tr B-Funf 52:471–488
10. Kumaresan T, Joshi J (2016) Effect of impeller design on the flow pattern and mixing in stirred tanks. Chem Eng J 115:173–193

11. Li LC, Xu B (2017) CFD simulation of local and global mixing time in an agitated tank. Chin J Mech Eng-En 30:118–126
12. Liu J, Luo FH, Lin XY, Ye T (2020) CFD Prediction with Eulerian/Eulerian Approach of SO_2 Absorption from Flue Gases in Bubble-Dispersion Tower. Arab J Scieng 45:7621–7634
13. Liu MS, Hohenshil A, Gadikota G (2021) Integrated CO_2 Capture and Removal via Carbon Mineralization with Inherent Regeneration of Aqueous Solvents. Energy Fuels 35:9
14. Malakhov AA, Toit MHd, Preez S, Pd, Avdeenkov AV, Bessarabov DG (2020) Temperature Profile Mapping over a Catalytic Unit of a Hydrogen Passive Autocatalytic Recombiner: An Experimental and Computational Fluid Dynamics Study. Energy Fuels 34:11637–11649
15. Mauro C, Massimo B, Marianna M, Guido B, Paolo C, Andrea CS (2010) Formulation design for optimal high-shear wet granulation using on-line torque measurements. Int J Pharmaceut 387:48–55
16. Mayoral MC, Andres JM, Gimeno MP (2013) Optimization of mineral carbonation process for CO_2 sequestration by lime-rich coal ashes. Fuel 106:448–454
17. Meng W, Sui FG, Hao XF, Zhang SP, Jiang Y, Wu SB, Zhang TJ, Feng YL (2022) Thermodynamic characteristics and mineral dissolution model of the H_2O-CO_2-$CaCO_3$-Albite-SiO_2 system in sedimentary basins. Fuel 308:121992
18. Miao ED, Zheng Xf, Xiong Z, Zhao YC, Zhang JY (2022) Kinetic modeling of direct aqueous mineral carbonation using carbide slag in a stirred tank reactor. Fuel 315:122837
19. Mondal BK, Bandyopadhyay SS, Samanta AN (2017) Kinetics of CO_2 Absorption in Aqueous Hexamethylenediamine Blended N-Methyldiethanolamine. Ind Eng Chem Res 56:14902–14913
20. Moradkhani H, Izadkhah M, Navideh A, Experimental (2017) Study of Oxygen Mass Transfer Coefficient in Different Impeller Configurations and Operational Conditions of a Two-Phase Partitioning Bioreactor. Appl Biochem Biotechnol 181:710–724
21. Pan SY, Chen YH, Fan LS, Kim H, Gao X, Ling TC, Chiang PC, Pei SL, Gu GW (2020) CO_2 mineralization and utilization by alkaline solid wastes for potential carbon reduction. Nat Sustain 3:399–405
22. Pham HH, Lim SH, Go KS, Nho NS, Kwon EH, Kim KH, Lim Y, Ryu HJ, Part SY (2022) Modeling and simulation of a bench-scale bubble column reactor for slurry phase hydrocracking of vacuum residue. Fuel 310:122481
23. Ranade VV, Joshi JB (1989) Flow generated by pitched blade turbines I: measurements using laser doppler a anemometer. Chem Eng Commun 81:197–224
24. Rigopoulos S, Jones A (2003) Modeling of Semibatch Agglomerative Gas-Liquid Precipitation of $CaCO_3$ in a Bubble Column Reactor. Ind Eng Chem Res 42:6567–6575
25. Raj K, Ramadan A, Saeed S (2020) Experiments and CFD modelling for two phase flow in a vertical annulus. Cem Eng Res Des 153:201–211
26. Song S, Zhou G, Duan JJ, Sun B, Wang YM (2021) CFD simulation of multi-phase and multi-component diffusion of air-dust-gas in a fully mechanized mining face. Environ Sci Pollut Res 7:1–16
27. Tatterson GB, Morrison GL (1987) Effect of tank to impeller diameter ratio on flooding transition for disc turbines. Aiche J 33:1751–1753

28. Wang JY, Zhong M, Wu PF, Wen SK, Huang L, Ning P (2021) P. A Review of the Application of Steel Slag in CO_2 Fixation, Chembioeng. Rev 8:189–199
29. Wang XT, Cui BY, Wei DZ, Song ZG, He Y, Bayly AE (2021) CFD simulation of tailings slurry thickening in a gravity thickener. Powder Technol 392:639–649
30. Wu Q, Wang S, Zhang K, He Y (2021b) Assessment of heat transfer performance in a swirling fluidized bed with binary mixture. Appl Therm Eng 194:117128
31. Wu MY, Hu XM, Zhang Q, Lu W, Zhao YY, He ZL (2020) Study on preparation and properties of environmentally-friendly dust suppressant with semi-interpenetrating network structure. J Cclean Prod 259:120870
32. Wu MY, Liang YT, Zhao YT, Wang W, Hu XM, Tian FC, He ZL, Li YS, Liu TY (2021a) Preparation of new gel foam and evaluation of its fire extinguishing performance. Colloids Surf Physicochem Eng Asp 629:127443
33. Wylock C, Larcy A, Colinet P, Cartage T, Hault B (2010) Direct numerical simulation of the CO_2 transfer from spherical bubbles to $NaHCO_3$ and Na_2CO_3 aqueous solutions with clean and fully contaminated interface. Colloids Surf Physicochem Eng Asp 365:28–35
34. Yang J, Ma LP, Liu HP, Wei Y, Keomounlath B, Dai QX (2019) Thermodynamics and kinetics analysis of Ca-looping for CO_2 capture: Application of carbide slag. Fuel 242:1–11
35. Yuan Y, Lu W, Cheng WM, Qi GS, Hu XM, Su H, Wang MJ, Zhang MY, Liang YT (2022) Method for rapid mineralization of CO_2 with carbide slag in the constant-pressure and continuous-feed way and its reaction heat. Powder Technol 398:117148
36. Zhang L, Yin YL, Li L, Wang F, Song QB, Zhao N, Xiao FK, Wei W (2016) Numerical Simulation of CO_2 Adsorption on K-Based Sorbent. Energy Fuels 30:4283–4291
37. Zuo ZJ, Gong SG, Xie G (2020) Numerical investigation of granular mixing in an intensive mixer: Effect of process and structural parameters on mixing performance and power consumption. Chin J Chem Eng 32:1004–1954

Figures

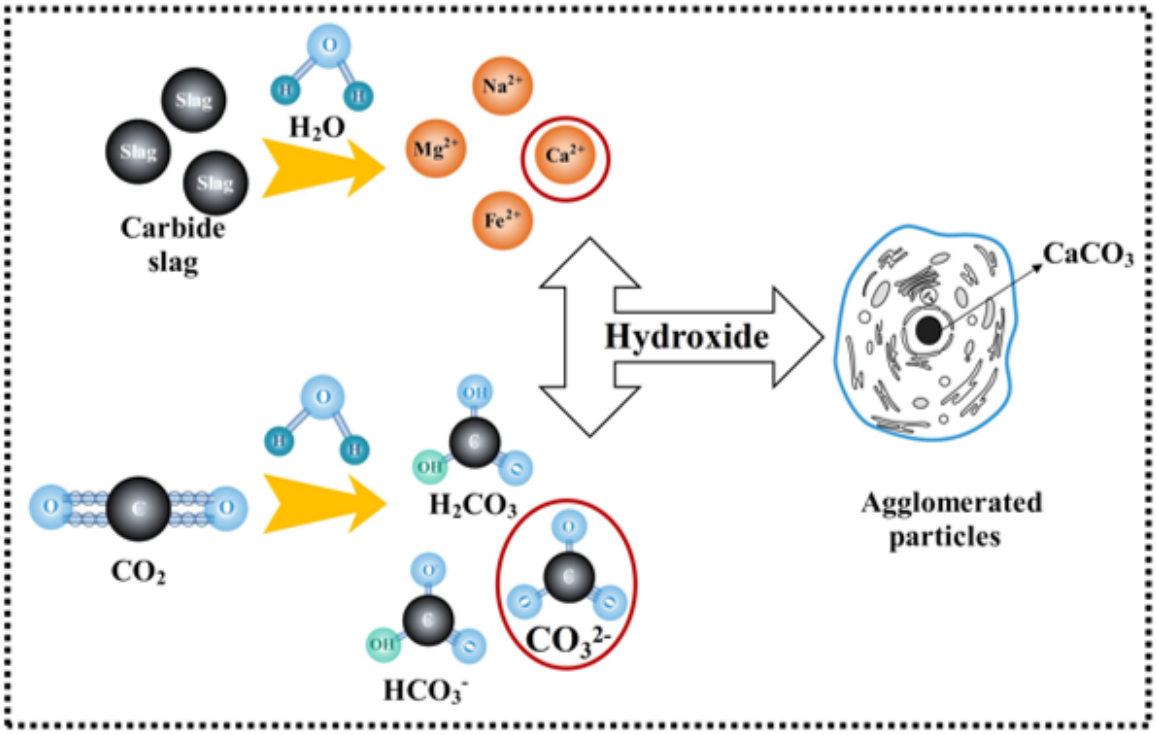

Figure 1

Schematic of instantaneous mass transfer near the gas-slurry interface of carbide slag slurry.

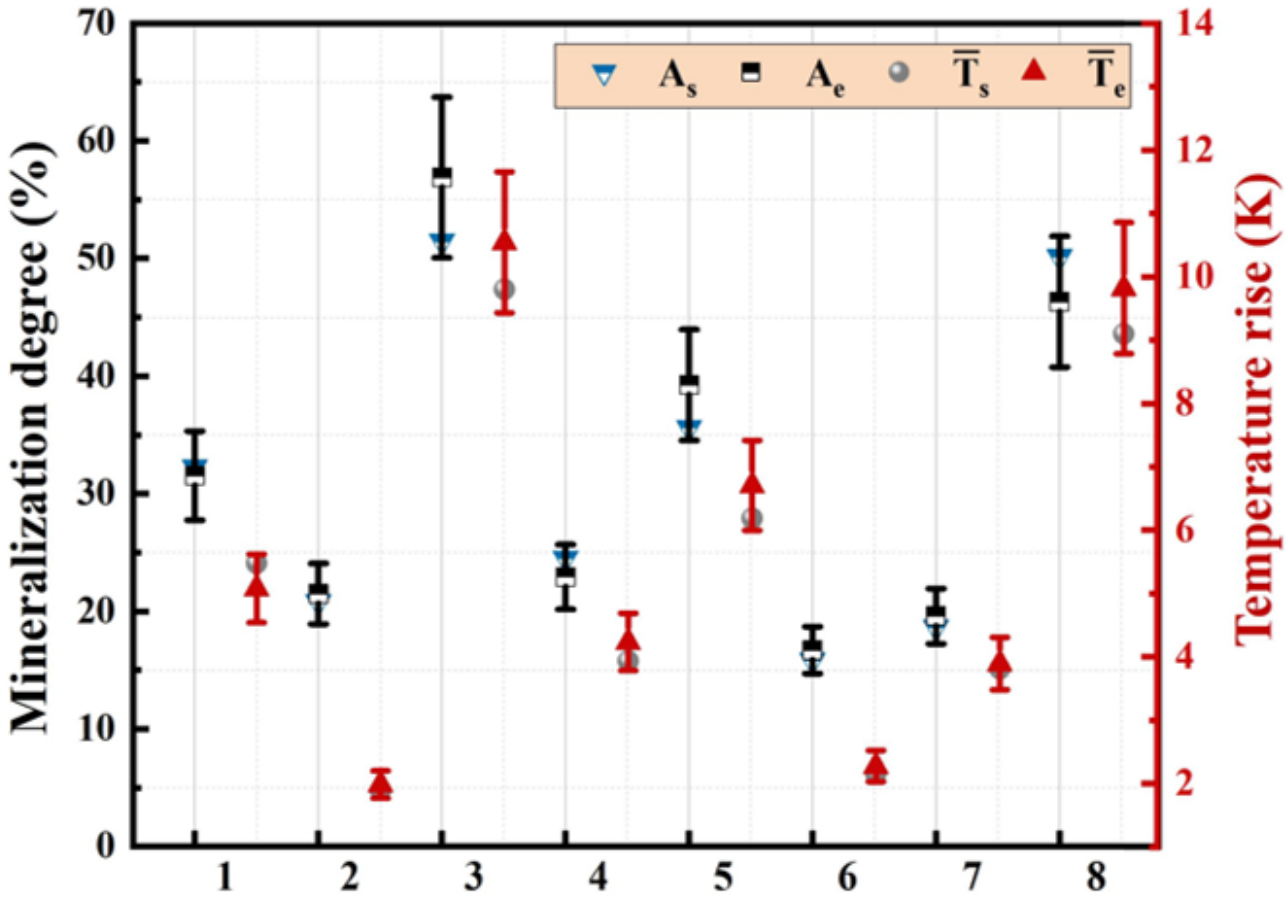

Figure 2

Comparison of data obtained in the experiment and numerical simulation.

Note: A_s and A_e are mineralization degrees in the numerical simulation and the experiment, respectively;`$T_s$ and`T_e are temperature increases in the numerical simulation and the experiment, respectively.

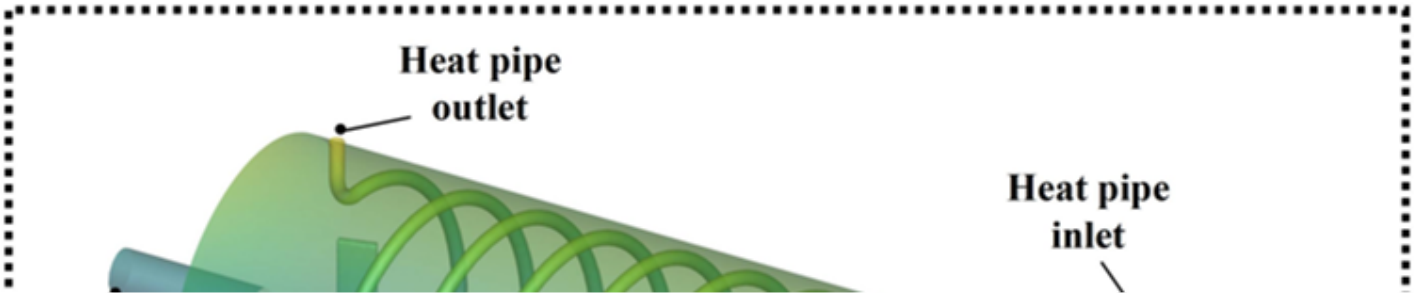

Figure 3

3D physical model of mixing device.

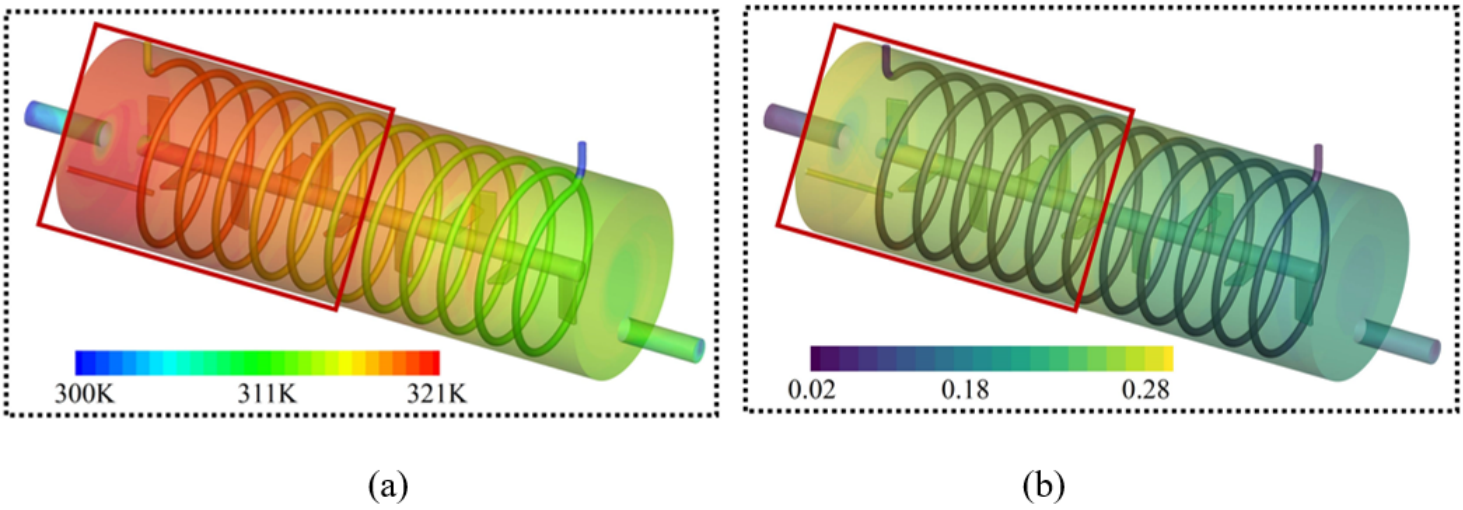

Figure 4

Nephograms of $CaCO_3$ concentration and temperature distribution (after the mass of $CaCO_3$ at the outlet stabilized).

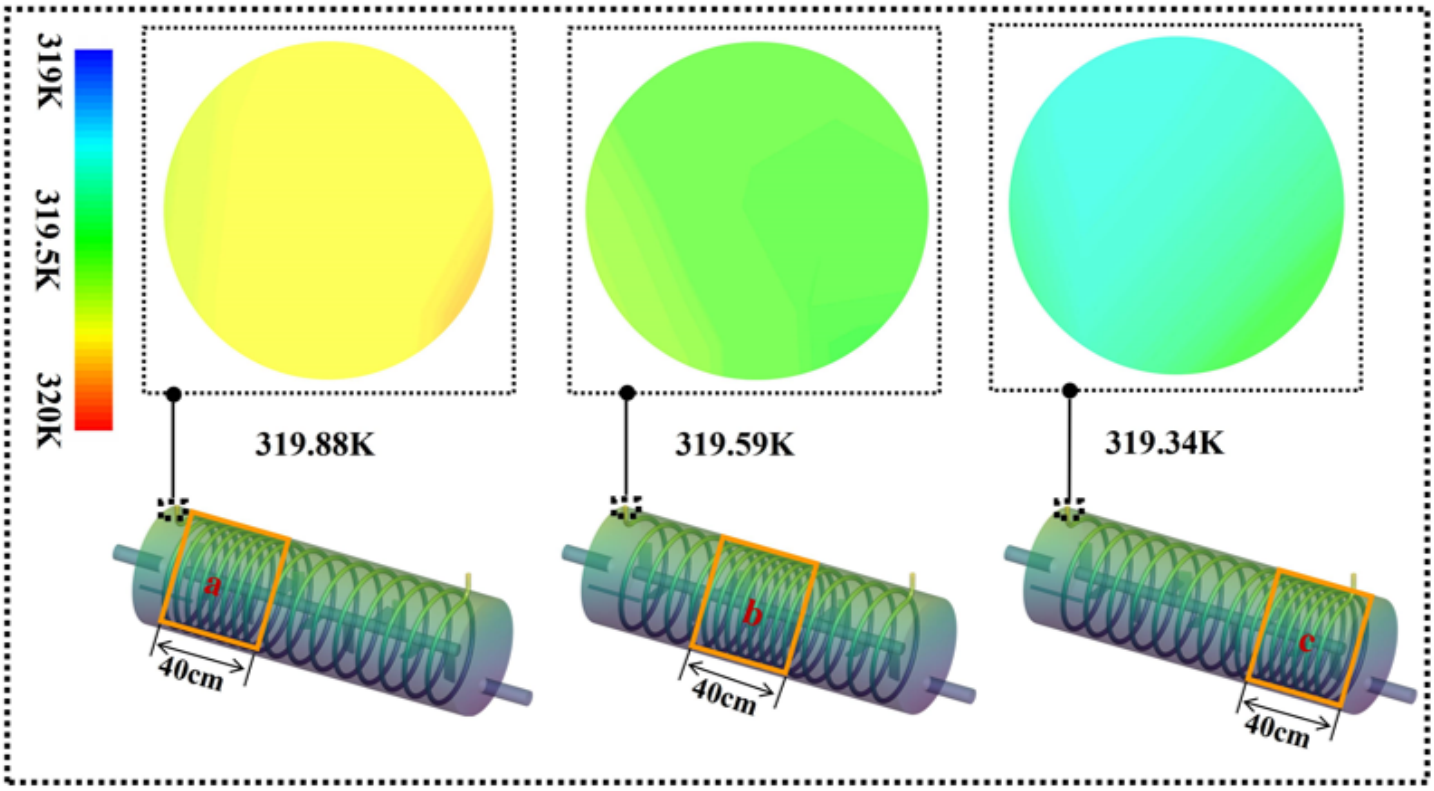

Figure 5

Cloud picture of water temperature at the mouth of heat pipe with different winding densities.

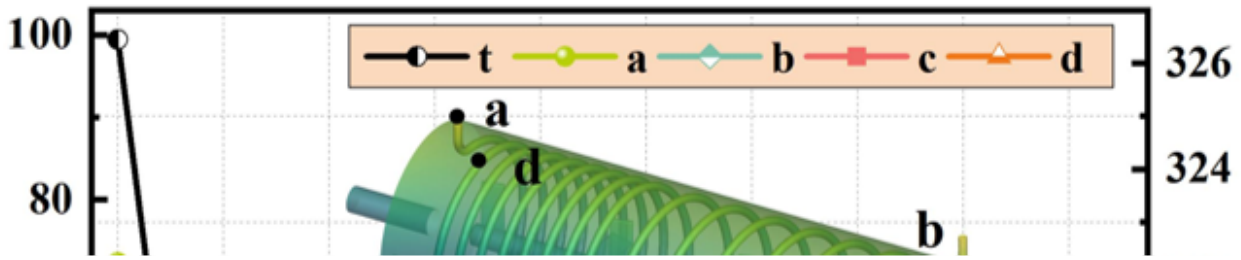

Figure 6

Relationship between time, temperature, and flow velocity.

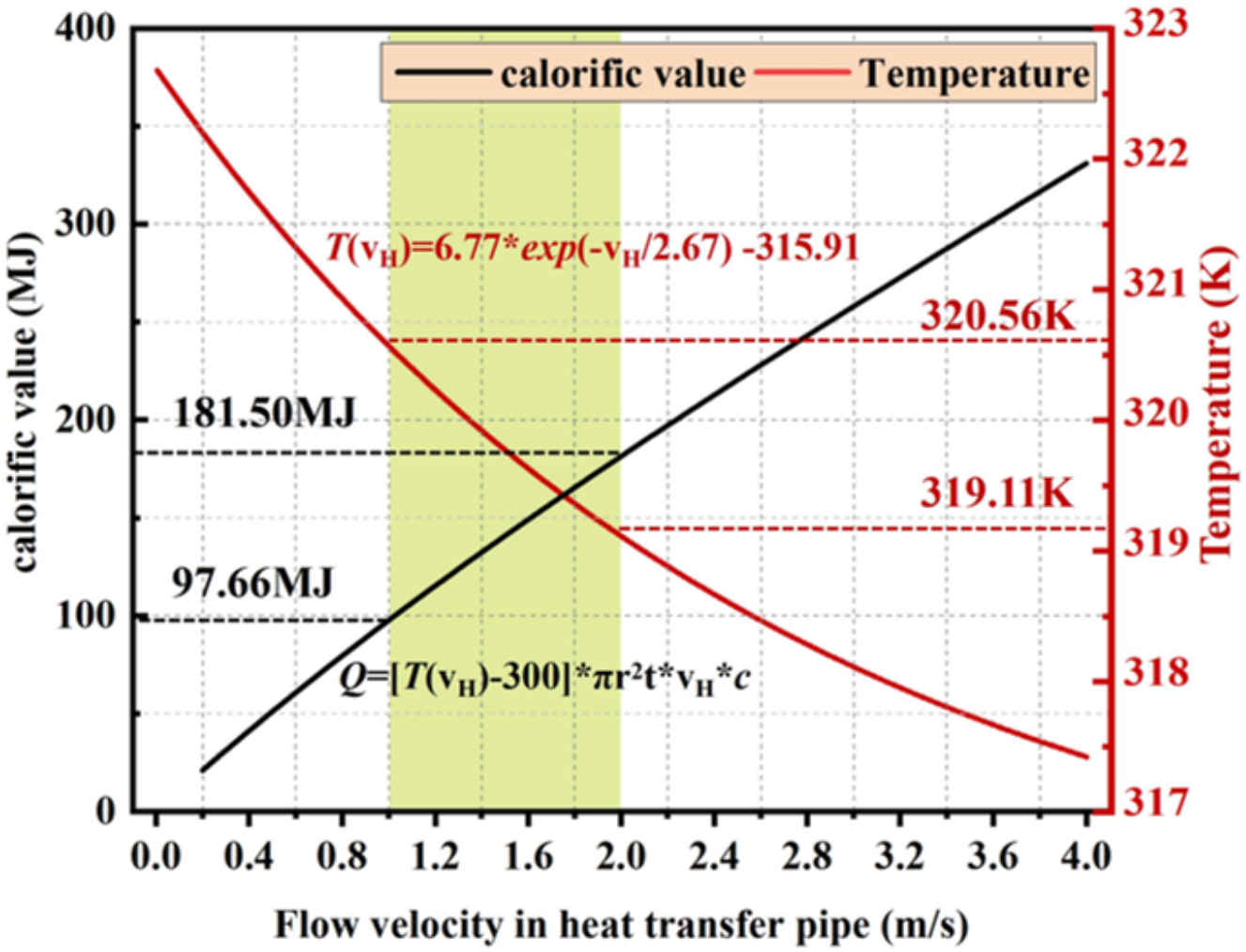

Figure 7

Relationship between reaction heat and flow velocity extracted by heat pipe within 1 h.